Antarctic and Southern Ocean influences on Late Pliocene global cooling

Robert McKay[a,1], Tim Naish[a], Lionel Carter[a], Christina Riesselman[b,2], Robert Dunbar[c], Charlotte Sjunneskog[d], Diane Winter[e], Francesca Sangiorgi[f], Courtney Warren[g], Mark Pagani[g], Stefan Schouten[h], Veronica Willmott[h], Richard Levy[i], Robert DeConto[j], and Ross D. Powell[k]

[a]Antarctic Research Centre, Victoria University of Wellington, PO Box 600, Wellington 6140, New Zealand; [b]Department of Geological and Environmental Sciences, Stanford University, Stanford, CA 94305; [c]Department of Environmental Earth Systems Science, Stanford University, Stanford, CA 94305; [d]Antarctic Marine Geology Research Facility, Florida State University, Tallahassee, FL 32306; [e]Rhithron Associates, Inc, Missoula, MT 59804; [f]Department of Earth Sciences, Faculty of Geosciences, Laboratory of Palaeobotany and Palynology, Utrecht University, U3584 CD Utrecht, The Netherlands; [g]Department of Geology and Geophysics, Yale University, New Haven, CT 06520; [h]NIOZ Royal Netherlands Institute for Sea Research, Department of Marine Organic Biogeochemistry, 1790 AB Den Burg, Texel, The Netherlands; [i]GNS Science, Lower Hutt 5040, New Zealand; [j]Department of Geosciences, University of Massachusetts, Amherst, MA 01003; and [k]Department of Geology and Environmental Geosciences, Northern Illinois University, DeKalb, IL 60115

Edited by* James P. Kennett, University of California, Santa Barbara, CA, and approved February 28, 2012 (received for review August 2, 2011)

The influence of Antarctica and the Southern Ocean on Late Pliocene global climate reconstructions has remained ambiguous due to a lack of well-dated Antarctic-proximal, paleoenvironmental records. Here we present ice sheet, sea-surface temperature, and sea ice reconstructions from the ANDRILL AND-1B sediment core recovered from beneath the Ross Ice Shelf. We provide evidence for a major expansion of an ice sheet in the Ross Sea that began at ∼3.3 Ma, followed by a coastal sea surface temperature cooling of ∼2.5 °C, a stepwise expansion of sea ice, and polynya-style deep mixing in the Ross Sea between 3.3 and 2.5 Ma. The intensification of Antarctic cooling resulted in strengthened westerly winds and invigorated ocean circulation. The associated northward migration of Southern Ocean fronts has been linked with reduced Atlantic Meridional Overturning Circulation by restricting surface water connectivity between the ocean basins, with implications for heat transport to the high latitudes of the North Atlantic. While our results do not exclude low-latitude mechanisms as drivers for Pliocene cooling, they indicate an additional role played by southern high-latitude cooling during development of the bipolar world.

glacial history | West Antarctic Ice Sheet | Late Neogene | paleooceanography | paleoclimate

The development of the first continental-scale ice sheet on Antarctica occurred at ∼34 Ma, coincident with a ∼1.5‰ increase in benthic foraminiferal $\delta^{18}O$ (1, 2), which is interpreted as a 4 °C cooling in deep ocean temperature (3) with 80 m of sea level equivalent ice volume on the Antarctic continent (4, 5). Direct geological evidence of a continental-scale ice sheet calving at the coastline by the earliest Oligocene came from ice-rafted debris in ocean drill cores from Prydz Bay (6, 7) and marine grounding-line deposits in Western Ross Sea drill cores (8). Proximal geological drill cores (9) and high-resolution deep-sea $\delta^{18}O$ (10) records imply the existence a dynamic and highly variable, orbitally paced East Antarctic Ice Sheet (EAIS) that drove global sea-level changes of ∼40 m (11) up until ∼14 Ma. A ∼1.2‰ increase in benthic foraminiferal $\delta^{18}O$ at ∼14 Ma and cooling of Southern Ocean surface waters by up to 7 °C is associated with the development of a more permanent EAIS (1, 12, 13). Terrestrial glacial deposits at high elevations in the Transantarctic Mountains (TAM) indicate a transition from wet-based to dry-based glaciation at this time, and using the preservation of delicate terrestrial plant fossils, ancient landscapes, and volcanic ashes, it has been argued that the volume of the EAIS remained relatively stable since ∼14 Ma (14, 15). While terrestrial glacial and glaciomarine deposits indicate marine incursions into fjords coupled with thinning and recession of the low elevation parts of the EAIS along Western Ross Sea and in Prydz Bay during the Pliocene (16, 17), widespread deglaciation of the EAIS at this time (18) is unsupported by ice sheet models (19, 20), benthic $\delta^{18}O$ records (21) and glacial deposits at high elevation in the TAM (22).

The development of an ephemeral West Antarctic Ice Sheet (WAIS) is thought to have occurred around 34 Ma (5) coincident with the first ice sheets in East Antarctica, but it was not a permanent feature until much later (23). Glacial unconformities observed in seismic profiles in the central Ross Sea, correlated to dated horizons in Deep Sea Drilling Project Site 270, indicate that periods of an extensive grounded marine ice sheet within the Ross Sea embayment have occurred since the Early Miocene (24). During the warmest intervals of the Pliocene (4.5–3.0 Ma) Earth's average surface temperature was ∼2–3 °C warmer than present, atmospheric pCO_2 was ∼400 ppmv, and equator to pole temperature gradients were weaker (25–27). During this peak Pliocene warmth, the largely marine-based WAIS and the Greenland Ice Sheet were reduced in extent (19, 28, 29) and global sea level is estimated to have been between 5–40 m above present with most reconstructions converging on 20–25 m (30). Subsequent cooling, which led to the onset of major Northern Hemispheric glaciation by ∼2.7 Ma (31), has been variously attributed to declining pCO_2 (32), changing orbital geometries (33), tectonic influences (34), increased oceanic stratification and precipitation in northern high latitudes (35), and reduced zonal sea-surface temperature (SST) gradients in the equatorial Pacific Ocean (36). Until now, the role of Antarctica in Late Pliocene global cooling has been unclear. The Antarctic Drilling Program's (ANDRILL) AND-1B core contains a series of well-dated sedimentary cycles documenting ice sheet advance and retreat that correlate with the global marine oxygen isotope and southern, high-latitude insolation time series (Fig. 1) (19, 28).

Here, we describe a major phase of ice sheet expansion and cooling in coastal Antarctic waters at ∼3.3 Ma following a ∼1.2 Myr-long period of warmer-than-present marine conditions accompanied by a diminished marine-based ice sheet in the Ross Embayment during the Early Pliocene (∼4.5–3.4 Ma). This cooling involved the expansion of the Antarctic ice sheets onto the continental shelf, increased sea ice extent and duration, and altered Southern Ocean circulation. Our multiproxy dataset

Author contributions: R.M., T.N., and R.L. designed research; R.M., T.N., L.C., C.R., R. Dunbar, C.S., D.W., F.S., C.W., M.P., S.S., V.W., and R.D.P. performed research; R.M., T.N., L.C., C.R., R. Dunbar, C.S., D.W., F.S., C.W., M.P., S.S., V.W., R.L., R. DeConto, and R.D.P. analyzed data; and R.M., T.N., L.C., and C.R. wrote the paper.

The authors declare no conflict of interest.

*This Direct Submission article had a prearranged editor.

[1]To whom correspondence should be addressed. E-mail: robert.mckay@vuw.ac.nz.

[2]Present address: Eastern Geology and Paleoclimate Science Center, US Geological Survey, Reston, VA 20192.

This article contains supporting information online at www.pnas.org/lookup/suppl/doi:10.1073/pnas.1112248109/-/DCSupplemental.

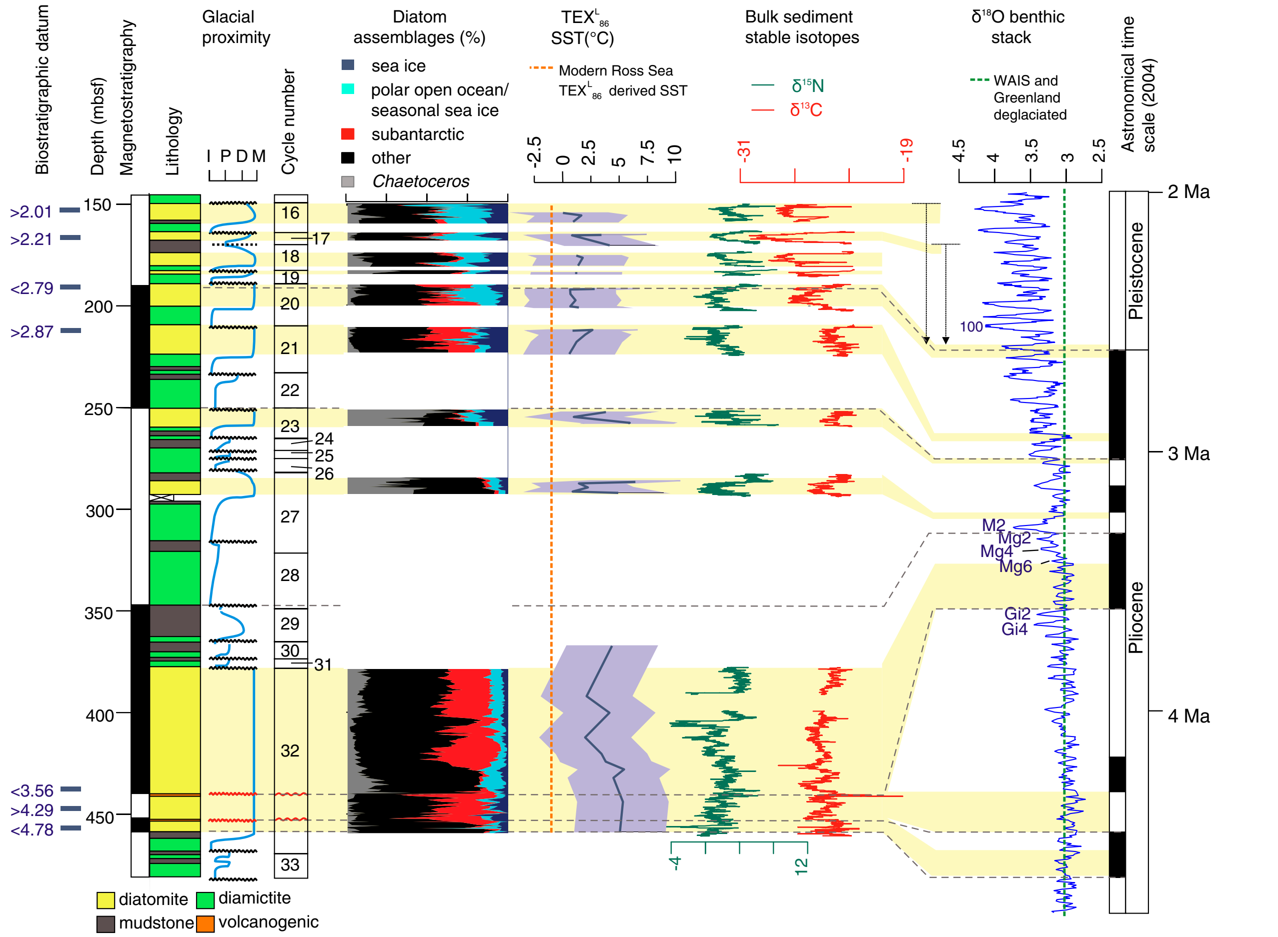

Fig. 1. Summary stratigraphic log of lithofacies in AND-1B. The glacial proximity curve is based on interpretation of the lithofacies and tracks the relative position of the grounding line [ice-contact (I), ice-proximal (P), ice-distal (D), and marine (M)], providing a proxy for ice-sheet extent (28). Chronostratigraphy is derived by magnetostratigraphy, constrained by biostratigraphy and tephrochronology (28). Diatom assemblages, TEX^L_{86} derived SST (with light purple calibration error envelope), and bulk sediment stable isotope data are from interglacial deposits, and record a cooling trend that is coincident with increased variance toward glacial values in the global $\delta^{18}O$ benthic stack (42).

indicates: (*i*) a progressive increase in ice sheet extent and variability, and reduced glacial meltwater, and (*ii*) a general cooling of the coastal Antarctic seas based on evidence from sedimentary facies, diatom assemblages, TEX^L_{86} (tetraether index of lipids consisting of 86 carbon atoms) sea-surface temperature reconstructions, and $\delta^{13}C$ and $\delta^{15}N$ of bulk sedimentary organic matter.

Results

AND-1B was drilled beneath the McMurdo Ice Shelf, an extension of the Ross Ice Shelf at its northwest margin. The provenance of clasts within subglacially deposited diamictites in AND-1B is consistent with transport by glacial ice from EAIS outlet glaciers to the south of the drill site (37), indicating deposition by grounded ice sheets within the Ross Embayment. Ice sheets that occupied the Ross Embayment and the AND-1B drill site during past glacial maxima were grounded several hundreds of meters below sea level and separated from the land-based sector of the EAIS by the TAM. Glacial retreat of these marine ice sheets is considered to be controlled by variations in ocean temperature and marine ice sheet instability processes associated with the reverse bed slope of the Ross Sea continental shelf (19, 38). This implies that, on glacial to interglacial timescales, once retreat was initiated for past configurations of the ice sheet, it was likely to have been widespread across the Ross Embayment, similar to the patterns documented for the last deglaciation (e.g., 39, 40). Therefore, we argue that the AND-1B record represents the overall state of the marine-based ice sheet in the Ross Embayment, and that the conditions that led to open water deposits at this location also require partial to complete collapse of the WAIS (19, 28).

In AND-1B, advances and retreats of the ice sheet grounding line (Fig. 1) are constrained by glaciomarine cyclic stratigraphy (28, 41). Each cycle begins with a sheared glacial surface of erosion (*SI Text*), overlain by subglacial and ice-proximal glaciomarine diamictites (poorly sorted deposits of gravel, sand, and mud), mudstones, and sandstones, passing upward into interglacial diatomites deposited under open-ocean conditions. During glaciations, the ice sheets had laterally extensive marine termini that extended beyond the AND-1B drill site onto the Ross Sea continental shelf (28). In general, our glacial proximity curve (Fig. 1) shows that WAIS expansion into the Ross Sea occurred during the Late Pliocene and Early Pleistocene when benthic marine $\delta^{18}O$ was more positive than Holocene values (42) and ice volumes exceeded the modern Antarctic volume of 27×10^6 km^3.

Grounding-line oscillations are absent in AND-1B during a composite interval referred to as Cycle 32 (4.6–3.4 Ma; Fig. 1), when ~80 m of diatomite was deposited (Fig. 1). The upper 60 m of diatomite accumulated between 3.6–3.4 Ma, when some of the lowest ice volumes and highest sea levels of the Pliocene occurred based on correlation to the benthic $\delta^{18}O$ stack (28, 42). Below the 60 m section, a hiatus of ~0.6 million years is associated with a debris flow of volcanic-rich diatomaceous sediment ~1 m-thick and a carbonate-cemented diatomite ~0.6 m-thick, which overlies 20 m of uncemented diatomite containing a shorter-duration hiatus at ∼453 m below seafloor (Fig. 1). These hiatuses represent nonglacial erosion or nondeposition, possibly due to currents invigorated by a modest ice sheet expansion that did not override the AND-1B drillsite (43). Ice sheet retreat in the Ross Embayment was also accompanied by retreat of the EAIS marine margin, as recorded from Prydz Bay at 4.7–4.3 Ma (16).

Although many of the diatom taxa in the Pliocene-early Pleistocene interval of AND-1B are now extinct, numerous species are still extant. Based on the present-day areal distribution of the species in the Southern Ocean (44–46), and therefore their sensitivity to modern SST and sea ice extent as it exists today (43, 47), we have grouped assemblages of extant diatom species preserved in AND-1B into three ecologically circumscribed categories. We term these groups "subantarctic," "polar open ocean and seasonal sea ice tolerant," and "sea ice" (*SI Text*). Only two extinct species are included; *Rouxia antarctica* and *Shionodiscus tetraoestrupii* are assigned to the "polar open ocean and seasonal sea ice tolerant" and "subantarctic" groups, respectively.

Diatom assemblages in the lower part of Cycle 32 contain abundant "subantarctic" flora that today live north of the Polar Front, whereas taxa that today occur south of the Polar Front, the "polar open ocean and seasonal sea ice tolerant" group, are a relatively minor constituent (Fig. 1). Combined with the very low abundance of diatom taxa that have maximum abundances in the modern zone of seasonal sea ice (Fig. 1), this indicates that sea ice was either absent or restricted to coastal areas during this prolonged period of ice sheet withdrawal in the Ross Embayment (43). Furthermore, δ^{13}C and δ^{15}N curves from Cycle 32 (Fig. 1) show low variance and limited coherence, indicating that Ross Sea surface conditions were substantially different from modern conditions and suggesting relatively invariant and moderate levels of summer productivity. In the modern Ross Sea, water column particulates and sea floor sedimentary organic matter display more negative δ^{13}C values in the deeply mixed polynya center than at the melt-stratified western margin (48), whereas δ^{15}N, which tracks nitrate utilization resulting from primary production, shows increased uptake of the total nitrate pool (more positive δ^{15}N values) in more stratified water (49).

Diatomite in Cycle 32 is overlain by four progressively more ice-proximal sequences (Cycles 31–28) containing diamictites and their associated glacial surfaces of erosion, which represent the first of two major cooling steps in the Late Pliocene section of the AND-1B core. These four cycles formed during a 0.8‰ increase in benthic δ^{18}O during glacial intervals, and correspond to an increase in modeled Antarctic ice volume from +7 m to −1 m equivalent sea-level relative to present (19). The base of Cycle 28 coincides with the base of the Mammoth Subchron at ∼3.3 Ma (Fig. 1). This surface is directly overlain by a ∼20 m thick diamictite deposited at the grounding zone during the glacial advance associated with Marine Isotope Stage (MIS) M2, the largest positive δ^{18}O excursion in the Early Pliocene (Fig. 1). The MIS M2 glaciation marks the beginning of a long-term trend toward progressively more positive δ^{18}O excursions culminating in MIS 100 at ∼2.5 Ma (Fig. 1). Subglacial sediments incorporated in Cycles 31–28 are the first evidence for grounded ice in the Ross Sea after ∼1 million years of open ocean conditions, and mark the termination of significantly warmer than present conditions in southern high latitudes. Subsequent glacial/interglacial grounding-line oscillations between 3.3–2.0 Ma (Cycles 27 to 16) reflect orbitally paced advance and retreat of a marine-based ice sheet across the AND-1B drill site. An up-core transition into cycles with successively thinner terrigenous glaciomarine facies (e.g., mudstone) between subglacial and open-ocean facies occurs in units between Cycles 32 and 21 (Fig. 1). This observation implies a reduction in subglacial meltwater outwash during glacial retreat, and reflects progressive cooling and drying of the subglacial regime from 3.3 to 2.9 Ma.

"Subantarctic" taxa are rare in the diatom assemblages of Cycles 27 and 23 (∼3.2 and 3.0 Ma; Fig. 1), and together with increased abundances of *Chaetoceros* resting spores suggest the occurrence of spring blooms in a well-stratified upper ocean influenced by seasonal sea ice melt. The abundance of the "subantarctic" assemblage increases again in Cycles 21–20 (∼3.0 to 2.6 Ma) but "polar open ocean and seasonal sea ice tolerant" and "sea ice" taxa also increase significantly. These observations indicate that while surface ocean conditions warmed relative to Cycles 27 and 23 they remained cooler than peak warmth recorded in Cycle 32 (Fig. 1). SSTs reconstructed from $\mathrm{TEX}_{86}^{\mathrm{L}}$ analysis (Fig. 1) support the cooling inferred from diatom assemblage analysis and facies interpretations despite recognized uncertainties of ±4 °C associated with the high-latitude $\mathrm{TEX}_{86}^{\mathrm{L}}$ calibration (50) (*SI Text*). The $\mathrm{TEX}_{86}^{\mathrm{L}}$-derived temperature for the inferred warm interglacial characterized by Cycle 32 is ∼5 °C in the lower half of this unit, but gradually cools to 2 °C in the later part of this interglacial. Cycle 32 contains species which are part of a "subantarctic" diatom-assemblage that occurs today between the Subantarctic and Polar Fronts where modern SSTs are ∼3–8 °C, which is broadly consistent with the $\mathrm{TEX}_{86}^{\mathrm{L}}$ derived-SST for Cycle 32.

Cycles 21 to 16 diatom assemblages contain a relatively large proportion of "polar open ocean or seasonal sea ice tolerant" and "sea ice" species (47). Today, these diatoms live in waters between the summer sea ice edge, where SSTs are as low as −1.5 °C, and the Polar Front, where SSTs rise to ∼3 °C (44–46). Although the abundance of extinct species in Pliocene AND-1B diatom assemblages hampers the development of a quantitative SST and sea ice reconstruction using modern analogues or transfer functions, the general trend of decreasing "subantarctic" species, and increasing "polar open ocean and seasonal sea ice tolerant" and "sea ice" species is consistent with the lower $\mathrm{TEX}_{86}^{\mathrm{L}}$-derived SSTs in the interglacials following Cycle 32.

In all diatomites younger than 3.3 Ma, δ^{13}C and δ^{15}N generally co-vary (Fig. 1), suggesting a shift toward modern oceanic conditions in the Ross Sea, which supports conclusions drawn from other environmental proxies outlined previously. Peak interglacial δ^{13}C is consistently less than −27‰ after ∼2.6 Ma (Cycle 20). Similar values today are only observed in the deeply mixed-central Ross Sea polynya (48), which is an important source area for sea ice and deep-water formation. Such negative values in the Pliocene and Pleistocene likely reflect enhanced polynya-style deep wind mixing of the surface ocean. In contrast, more positive δ^{13}C and δ^{15}N values at the start and end of interglacial periods suggest increased stratification due to sea ice melt in the absence of a well-developed polynya. A notable feature of the $\mathrm{TEX}_{86}^{\mathrm{L}}$ data in most AND-1B diatomites younger than 3.3 Ma is that the derived SSTs are ∼2–4 °C warmer during the glacial retreat and advance phases than during the middle of the interglacial (Fig. 1). As the TEX_{86} proxy is likely to be sensitive to variations in water column structure (*SI Text*), it may be influenced by meltwater processes. Increased stratification, and therefore warming of the upper water column, would be expected to occur when the ice sheets were more proximal to AND-1B or there was increased sea ice duration/extent. Such stratification is indicated by the more positive δ^{13}C and δ^{15}N values at the start and end of these interglacials (Fig. 1). However, during the peak interglacial the lower δ^{13}C and δ^{15}N values suggest a well-mixed water column, and therefore the $\mathrm{TEX}_{86}^{\mathrm{L}}$ temperatures would be expected to be more consistent with mixing of colder waters from the subsurface and temperatures of ∼0–2 °C (Fig. 1). A similar pattern has been noted in a TEX_{86} record from a Holocene diatom ooze in the Antarctic Peninsula, with TEX_{86}-derived SSTs 3–4 °C warmer during the deglacial (12–9 ka), compared to those later in the Holocene (<9 ka; 51), and is also attributed to increased meltwater stratification. Although there is uncertainty in the use of

TEX^{L}_{86} calibration to obtain absolute SST values in high polar latitudes (50), the general trend of TEX^{L}_{86} cooling in the Pliocene interval of AND-1B is consistent with the sedimentological, diatom, and stable isotope interpretations of cooling.

A significant cooling is represented by grounding-line advance and substantial erosion at the base of Cycle 20, with loss of up to ~300 kyrs of record immediately below the Gauss-Matuyama transition at 2.6 Ma (Fig. 1). The "subantarctic" diatom assemblage is mostly absent in the overlying diatomite of Cycle 19, and is replaced by taxa more consistent with the presence of sea ice or cold, open waters (47) (*SI Text*). Although AND-1B diatomites reveal marked Late Pliocene cooling, they do not record the transition to late Pleistocene-Holocene Ross Sea diatom assemblages, which most likely occurred during additional cooling steps sometime after 2.0 Ma (52, 53), possibly after 1.0 Ma when the ice sheets in the Ross Embayment cooled to such extent that the Ross Ice Shelf, rather than marine conditions, persisted at the AND-1B drillsite throughout interglacial periods (41, 47). Rather, the Late Pliocene diatom assemblage in AND-1B likely represents a cooling of the surface ocean that favored increased duration and extent of sea ice into the summer months.

Discussion

Ice sheet expansion and development of sea ice in Antarctica's coastal regions between 3.3 and 2.6 Ma appear to be accompanied by major changes in the Southern Ocean that affected heat transport farther afield (Fig. 2). Foraminiferal $\delta^{13}C$ and $\delta^{18}O$ from tropical Atlantic sediments suggest only minor input of Antarctic deep waters above 3,000 m depth prior to 3.7 Ma, even during glaciations (54). This supports a strong Atlantic Meridional Overturning Circulation (AMOC) that enhanced the supply of North Atlantic Deep Water (NADW), and was accompanied by reduced Antarctic Bottom Water (AABW) and Lower Circumpolar Deep Water (LCDW) input, reflecting diminished Antarctic ice sheet extent. A decrease in benthic $\delta^{13}C$ during MIS Mg4 (~3.4 Ma) at Ocean Drilling Program (ODP) Site 925 (54) in the equatorial Atlantic, recording the first Late Pliocene expansion of AABW/LCDW and mixing with NADW at ~3,000 m depth. Stable isotopes and increased abundances of the benthic foraminifera *Nuttallides umbonifera* (55) highlight an increased northward influx of AABW/LCDW into the Atlantic Ocean between ~3.2–2.9 Ma (e.g., Figs. 2 and 3). This incursion presumably reflected enhanced bottom and deep water production in the Weddell Sea, Ross Sea, and other source areas following the MIS Mg4 to M2 glacial advances, and the subsequent polynya and sea ice development recorded in AND-1B (Fig. 1 and 2). At ~2.8 Ma, $\delta^{13}C$ of deep Southern Ocean water decreases significantly compared to the North Atlantic and Pacific Ocean (Fig. 2*C*; 56–58), which is attributed to reduced Southern Ocean ventilation due to increased sea ice cover and surface water stratification (56).

An observed increase in southern mid-latitude dust deposition after 2.8 Ma suggests enhanced atmospheric circulation, or an expanded dust source (59; Fig. 2*D*), and coincides with an increase in primary productivity at the Subantarctic Front (53) (Fig. 2*E*). This transition also appears to be associated with the development of polynya-style mixing and a higher abundance of the sea ice tolerant diatom group in the Ross Sea (Fig. 2*G*) and off the Antarctic Peninsula. The latter experienced declining opal production between ~3.2 Ma and 2.3 Ma as a consequence of a longer duration of summer sea ice and a resultant reduction in light availability (53) (Fig. 2*F*). We suggest that extensive Antarctic sea ice may have reduced the warming effect of the Southern Hemisphere subtropical gyres on high latitudes through northward migration of ocean fronts, including reducing the Agulhas inflow and its influence on the AMOC (e.g., Fig. 3) as has been inferred for Late Pleistocene glacial periods (60–62). Additionally, tectonic modification of the Indonesian Seaway be-

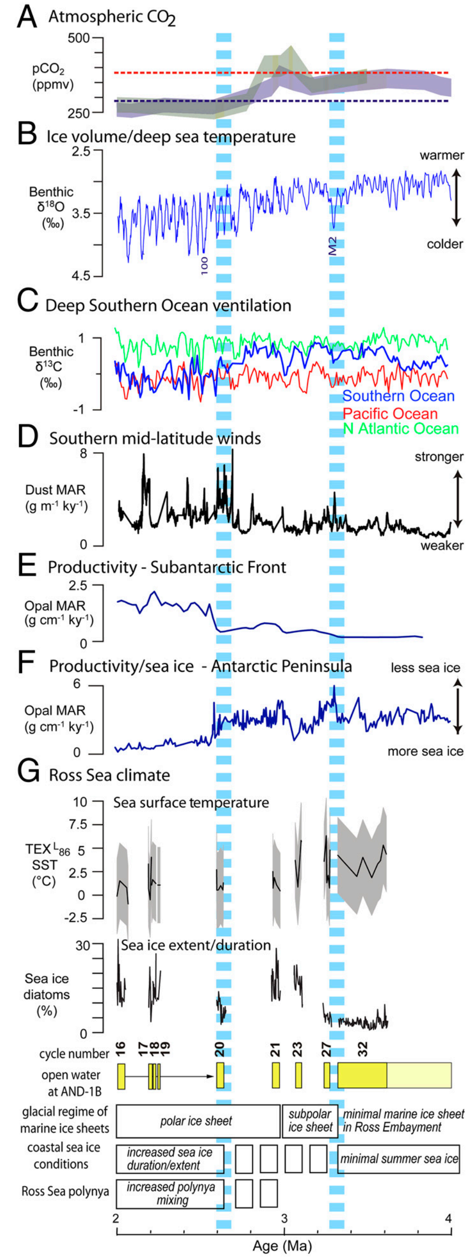

Fig. 2. Southern Hemisphere climate system feedbacks and responses, and their relationship to Antarctic climate evolution between 4–2 Ma. Steps in the deterioration of Pliocene climate at ~3.3 Ma and ~2.6 Ma are highlighted by blue dashed lines. (*A*) Atmospheric CO_2 concentration derived from boron- (purple) and alkenone- (green) based marine proxies (26), compared with present (red line) and preindustrial (blue line) concentrations. (*B*) Benthic foraminiferal $\delta^{18}O$ proxy for ice volume and temperature ($\delta^{18}O$; 42). (*C*) Influence of southern sourced bottom waters on deep ocean ventilation at ~2.8–2.6 Ma shown by comparison of benthic foraminiferal $\delta^{13}C$ records from South Atlantic/Southern Ocean ODP Sites 704/1090 (56), equatorial Pacific Ocean ODP Site 849 (57), and North Atlantic DSDP site 607 (58). (*D*) Atmospheric circulation (relative westerly wind strength) from dust mass accumulation rates for ODP Site 1090 (59). (*E*) Southern Ocean primary productivity based on biogenic opal mass accumulation rates at ODP Site 1091 shows a sharp increase coincident with increased windiness and nutrient supply by Fe-rich dust at ~2.6 Ma (53, 59). (*F*) Onset of Antarctic sea ice at ~2.6 Ma marked by a decline in primary productivity recorded in biogenic opal mass accumulation at Antarctic Peninsula ODP Site 1096 (53). (*G*) Summary of ocean, sea ice, and ice sheet evolution in Ross Embayment based on the AND-1B record. Note the cooling in SST and the return of periodic grounded ice sheets to western Ross Embayment occurs at ~3.3 Ma, ending a ~1.2 Ma period of relatively warm, ice free, open ocean conditions, and the appearance of sea ice and the development Ross Sea polynya between 3.2 and 2.6 Ma. Drill site locations are shown in Fig. 3.

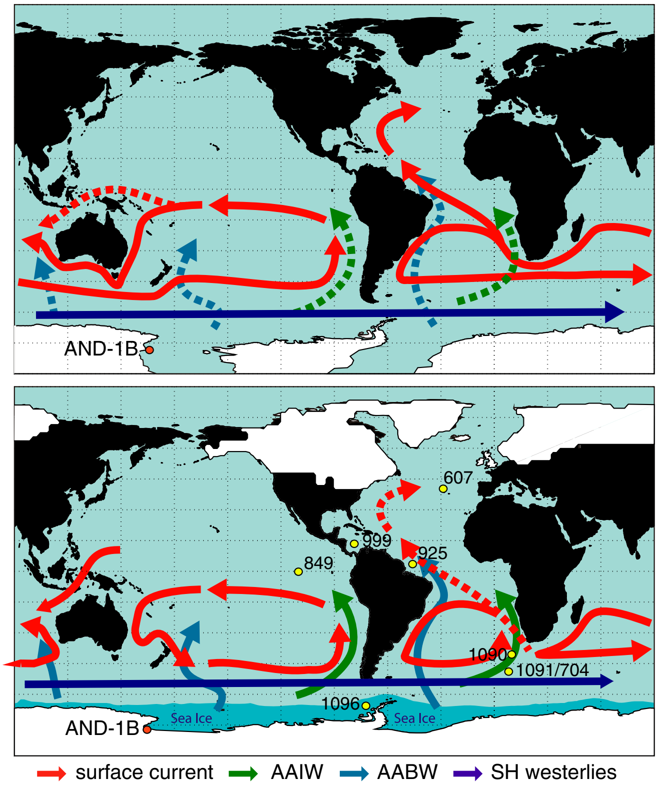

Fig. 3. Schematic representation of ocean surface circulation and intermediate/deep water mass formation responses to Late Pliocene Antarctic cooling. Dotted lines represent reduced water mass formation or current strength. (*Upper*) The warm Pliocene was characterized by a reduced WAIS volume and sea ice extent and duration during interglacials. Such conditions during Pleistocene glacial-interglacial transitions are associated with southward migration of Southern Ocean fronts (60, 61), allowing for greater connectivity of the Pacific, Indian, and Atlantic subtropical gyres, and may have promoted enhanced AMOC (61, 62). (*Lower*) Antarctic Ice Sheet expansion and sea ice growth in the Late Pliocene, and associated northward migration of the Southern Ocean frontal systems restricts water exchange between ocean basins, and reduces the AMOC (61). Increased sea ice extent during these steps resulted in increased AABW formation (55) (blue arrows) and the intensified frontal systems likely promoted AAIW and SAMW formation (66).

tween ~3–4 Ma potentially reduced and cooled the westward inflow of Pacific water into the Indian Ocean, in turn exacerbating the reduced heat transport via Agulhas leakage and heat transport to higher latitudes (34). The influence of upwelling NADW would also be reduced along the Antarctic margin, a process potentially enhanced by expanded ice sheets and sea ice. As noted earlier, such conditions favored local formation of AABW/LCDW, which along with a reduced AMOC would have affected the global heat transport.

Another consideration is that these ice sheet/sea ice/ocean changes between 3.3 and 2 Ma coincided with increased productivity and upwelling of cooler waters in the eastern equatorial Pacific (63) and the southeastern Atlantic (64) oceans. The intensification of the eastern Pacific upwelling and productivity at this time (65) has been associated with termination of "permanent El Niño-like" conditions in the Pacific Ocean, itself a potentially important global cooling mechanism (36). In the Southern Ocean, changes in wind fields have been linked to increased production of Antarctic Intermediate Water (AAIW) near the Polar Front, as postulated for the LGM (66). Thus, expansion of sea ice in the Southern Ocean may have driven increased upwelling of cooler water in the lower latitudes, with models simulating a potential 44% reduction of heat flux into the eastern equatorial Pacific under increased Southern Hemisphere sea ice (67).

Atmospheric teleconnections to equatorial regions and high northern latitudes, based on model simulations, indicate that major ice sheet and sea ice expansion in either hemisphere significantly alters the global Hadley circulation (68). Although the development of northern hemisphere ice sheets in the Late Pliocene complicates the exact nature of this feedback, altered Hadley circulation may initiate wholesale latitudinal shifts in the position of the Intertropical Convergence Zone, trade winds, and southern midlatitude westerlies—all of which influence wind-driven upwelling and the dynamics of frontal systems, and Southern Ocean ventilation rates (68, 69).

In conclusion, this reconstruction of Pliocene and Early Pleistocene Ross Sea climate and Antarctic ice sheets, based on new evidence from the AND-1B core, indicates a smaller WAIS, prolonged marine conditions in the Ross Embayment, and reduced sea ice extent and duration before 3.3 Ma. Subsequent Southern Ocean cooling and increased seasonal persistence of Antarctic sea ice occurred between 3.3 and 2.6 Ma, coinciding with a potential drawdown of atmospheric CO_2 from ~400 to ~280 ppm (Figs. 1 and 2*A*) (36). This cooling affected expansion of westerly winds and northward migration of ocean fronts in the Southern Ocean, likely restricting the warm Agulhas inflow into the Atlantic (61, 62). We suggest such a scenario contributed to a slowdown of the interhemispheric AMOC beginning after 3.3 Ma, and helped precondition the Northern Hemisphere for continental glaciation. Furthermore, ice-albedo and oceanic/atmospheric feedbacks in both hemispheres, plus cooling in the upwelling zones of the eastern equatorial Pacific (36, 67) and Southeast Atlantic (64), would have further intensified cooling into the Pleistocene (52). Our reconstruction constrains the timing and nature of Late Pliocene cooling in the Southern Hemisphere and provides new evidence supporting the link between ice-sheet, sea ice, and oceanic processes from polar to equatorial latitudes. These boundary conditions and linkages provide a new context for numerical modeling and understanding of the global cooling that ultimately led to the bipolar-glacial world.

Material and Methods

AND-1B was described using standard sedimentological techniques to produce detailed stratigraphic logs (41). Diatom groupings are based on a synthesis of core top (modern) diatom assemblages in the Southern Ocean (44–46) with minor modifications (*SI Text*). $\delta^{13}C$ and $\delta^{15}N$ sediment samples were analyzed at the Stanford University Stable Isotope Laboratory. TEX^{L}_{86} was analyzed at Yale University and NIOZ Royal Netherlands Institute for Sea Research. Detailed methodology is provided as *SI Text*. Samples were provided by the Antarctic Marine Geology Research Facility, Florida State University.

ACKNOWLEDGMENTS. The scientific studies for ANDRILL are jointly supported by the US National Science Foundation, the NZ Royal Society of New Zealand Marsden Fund, the Italian Antarctic Research Programme, the German Research Foundation, and the Alfred Wegener Institute for Polar and Marine Research.

1. Shackleton NJ, Kennett JP (1975) Paleotemperature history of the Cenozoic and the initiation of Antarctic glaciation; oxygen and carbon isotope analyses in DSDP sites 277, 279, and 281. *Initial Reports of the Deep Sea Drilling Project* 29:743–755.
2. Coxall HK, Wilson PA, Palike H, Lear CH, Backman J (2005) Rapid stepwise onset of Antarctic glaciation and deeper calcite compensation in the Pacific Ocean. *Nature* 433:53–57.
3. Liu Z, et al. (2009) Global cooling during the Eocene-Oligocene climate transition. *Science* 323:1187–1190.
4. DeConto RM, et al. (2008) Thresholds for Cenozoic bipolar glaciation. *Nature* 455:652–656.
5. Wilson DS, Luyendyk BP (2009) West Antarctic paleotopography estimated at the Eocene-Oligocene climate transition. *Geophys Res Lett* 36:L16302.

6. Hambrey MJ, Ehrmann WU, Larsen B (1991) Cenozoic glacial record of the Prydz Bay continental shelf, East Antarctica. *Proc ODP Sci Results* 119:77–132.
7. Zachos JC, Breza JR, Wise SW (1992) Early Oligocene ice-sheet expansion on Antarctica: Stable isotope and sedimentological evidence from Kerguelen Plateau, southern Indian Ocean. *Geology* 20:569–573.
8. Barrett P (1989) Antarctic Cenozoic history from CIROS-1 Drill Hole, McMurdo Sound. *NZ DSIR Bull* 245:1–251.
9. Naish TR, et al. (2001) Orbitally induced oscillations in the East Antarctic ice sheet at the Oligocene/Miocene boundary. *Nature* 413:719–723.
10. Palike H, et al. (2006) Theheartbeat of the Oligocene climate system. *Science* 314:1894–1898.
11. Miller KG, et al. (2005) The phanerozoicrecord of global sea-Level change. *Science* 310:1293–1298.
12. Zachos J, Pagani M, Sloan L, Thomas E, Billups K (2001) Trends, rhythms, and aberrations in global climate 65 Ma to present. *Science* 292:686–693.
13. Shevenell AE, Kennett JP, Lea DW (2004) Middle Miocene southern ocean cooling and Antarctic cryosphereexpansion. *Science* 305:1766–1770.
14. Lewis A, Marchant D, Ashworth A, Hemming S, Machlus M (2007) Major middle Miocene global climate change: Evidence from East Antarctica and the Transantarctic Mountains. *Geol Soc Am Bull* 119:1449–1461.
15. Lewis AR, et al. (2008) Mid-Miocene cooling and the extinction of tundra in continental Antarctica. *Proc Natl Acad Sci USA* 105:10676–10680.
16. Hambrey MJ, McKelvey B (2000) Major Neogene fluctuations of the East Antarctic ice sheet: Stratigraphic evidence from the Lambert Glacier region. *Geology* 28:887–890.
17. Barrett PJ, Hambrey MJ (1992) Plio-Pleistocene sedimentation in Ferrar Fiord, Antarctica. *Sedimentology* 39:109–123.
18. Webb PN, Harwood DM, McKelvey BC, Mercer JH, Stott LD (1984) Cenozoic marine sedimentation and ice-volume variation on the East Antarctic craton. *Geology* 12:287–291.
19. Pollard D, DeConto RM (2009) Modelling West Antarctic ice sheet growth and collapse through the past five million years. *Nature* 458:329–332.
20. Dolan AM, et al. (2011) Sensitivity of Pliocene ice sheets to orbital forcing. *Palaeogeo Palaeoclimatol Palaeoecol* 309:98–110.
21. Kennett JP, Hodell DA (1993) Evidence for relative climatic Stability of Antarctica during the Early Pliocene: A marine perspective. *Geografiska Annaler Series A, Physical Geography* 75:205–220.
22. Denton GH, Sugden DE, Marchant DR, Hall BL, Wilch TI (1993) East Antarctic ice sheet sensitivity to Pliocene climatic change from a dry valleys perspective. *Geografiska Annaler Series A, Physical Geography* 75:155–204.
23. Kennett JP, Barker PF (1990) Latest Cretaceous to Cenozoic climate and oceanographic developments in the Weddell Sea, Antarctica: An ocean drilling perspective. *Proc ODP Sci Results* 113:937–960.
24. Bart PJ (2003) Were West Antarctic Ice Sheet grounding events in the Ross Sea a consequence of East Antarctic Ice Sheet expansion during the middle Miocene? *Earth Planet Sci Lett* 216:93–107.
25. Dowsett HJ, et al. (2010) The PRISM3D paleoenvironmental reconstruction. *Stratigraphy* 7:123–139.
26. Seki O, et al. (2010) Alkenone and boron-based Pliocene pCO_2 records. *Earth Planet Sci Lett* 292:201–211.
27. Brierley CM, et al. (2009) Greatly expanded tropical warm pool and weakened Hadley circulation in the Early Pliocene. *Science* 323:1714–1718.
28. Naish T, et al. (2009) Obliquity-paced Pliocene West Antarctic ice sheet oscillations. *Nature* 458:322–328.
29. Hill DJ, Dolan AM, Haywood AM, Hunter SJ, Stoll DK (2010) Sensitivity of the Greenland Ice Sheet to Pliocene sea surface temperatures. *Stratigraphy* 7:111–122.
30. Raymo ME, Mitrovica JX, O'Leary MJ, DeConto RM, Hearty PJ (2011) Departures from eustasy in Pliocene sea-level records. *Nat Geosci* 4:328–332.
31. Ravelo AC, Andreasen DH, Lyle M, Olivarez Lyle A, Wara MW (2004) Regional climate shifts caused by gradual global cooling in the Pliocene epoch. *Nature* 429:263–267.
32. Lunt DJ, Foster GL, Haywood AM, Stone EJ (2008) Late Pliocene Greenland glaciation controlled by a decline in atmospheric CO_2 levels. *Nature* 454:1102–1105.
33. Maslin MA, Li XS, Loutre M, Berger A (1998) The contribution of orbital forcing to the progressive intensification of northern hemisphere glaciation. *Quat Sci Rev* 17:411–426.
34. Cane MA, Molnar P (2001) Closing of the Indonesian seaway as a precursor to east African aridification around 3–4 million years ago. *Nature* 411:157–162.
35. Haug GH, et al. (2005) North Pacific seasonality and the glaciation of North America 2.7 million years ago. *Nature* 433:821–825.
36. Fedorov AV, et al. (2006) The Pliocene Paradox (mechanisms for a permanent El Nino). *Science* 312:1485–1489.
37. Talarico F, McKay R, Powell R, Sandroni S, Naish T (1974) Late Cenozoic oscillations of Antarctic ice sheets revealed by provenance of basement clasts and grain detrital modes in ANDRILL core AND-1B. *Glob Planet Change* 3:38–42 10.1016/j.gloplacha.2009.12.002.
38. Weertman J (1974) Deformation of floating ice shelves. *J Glaciology* 3:38–42.
39. Conway H, Hall BL, Denton GH, Gades AM, Waddington ED (1999) Past and future grounding-line retreat of the West Antarctic ice sheet. *Science* 286:280–283.
40. Shipp S, Anderson J, Domack E (1999) Late Pleistocene-Holocene retreat of the West Antarctic Ice-Sheet system in the Ross Sea: Part 1-Geophysical results. *Geol Soc Am Bull* 111:1486–1516.
41. McKay R, et al. (2009) The stratigraphic signature of the late Cenozoic Antarctic Ice Sheets in the Ross Embayment. *Geol Soc Am Bull* 121:1537–1561.
42. Lisiecki LE, Raymo ME (2005) A Pliocene-Pleistocene stack of 57 globally distributed benthic $\delta^{18}O$ records. *Paleoceanography* 20:PA1003.
43. Winter D, Sjunneskog C, Harwood D (2010) Early to mid-Pliocene environmentally constrained diatom assemblages from the AND-1B drillcore, McMurdo Sound, Antarctica. *Stratigraphy* 7:207–210.
44. Crosta X, Romero O, Armand LK, Pichon J (2005) The biogeography of major diatom taxa in Southern Ocean sediments: 2. Open ocean related species. *Palaeogeog Palaeoclimat Palaeoecol* 223:66–92.
45. Romero O, Armand L, Crosta X, Pichon J (2005) The biogeography of major diatom taxa in Southern Ocean surface sediments: 3 Tropical/Subtropical species. *Palaeogeog Palaeoclimat Palaeoecol* 223:49–65.
46. Armand LK, Crosta X, Romero O, Pichon J (2005) The biogeography of major diatom taxa in Southern Ocean sediments: 1. Sea ice related species. *Palaeogeog Palaeoclimat Palaeoecol* 223:93–126.
47. Sjunneskog C, Winter D A diatom record of late Pliocene cooling from the Ross Sea continental shelf, AND-1B, Antarctica. *Glob Planet Change*, in press.
48. Villinski JC, Dunbar RB, Mucciarone DA (2000) Carbon 13/Carbon 12 ratios of sedimentary organic matter from the Ross Sea, Antarctica: A record of phytoplankton bloom dynamics. *J Geophys Res* 105:14163–14172.
49. DiFiore PJ, Sigman DM, Dunbar RB (2009) Upper ocean nitrogen fluxes in the Polar Antarctic Zone: Constraints from the nitrogen and oxygen isotopes of nitrate,. *Geochem Geophys Geosyst* 10:Q11016.
50. Kim J, et al. (2010) New indices and calibrations derived from the distribution of crenarchaealisoprenoidtetraether lipids: Implications for past sea surface temperature reconstructions. *Geochimicaet Cosmochimica Acta* 74:4639–4654.
51. Shevenell AE, Ingalls AE, Domack EW, Kelly C (2011) Holocene Southern Ocean surface temperature variability west of the Antarctic Peninsula. *Nature* 470:250–254.
52. Martínez-Garcia A, Rosell-Melé A, McClymont EL, Gersonde R, Haug GH (2010) Subpolarlink to the emergence of the modern equatorial Pacific cold tongue. *Science* 328:1550–1553.
53. Hillenbrand C-D, Cortese G (2006) Polar stratification: A critical view from the Southern Ocean. *Palaeogeog Palaeoclimat Palaeoecol* 242:240–252.
54. Billups K, Ravelo AC, Zachos JC (1997) Early Pliocene deep-water circulation: Stable isotope evidence for enhanced northern component deep water. *Proc ODP Sci Results* 154:319–330.
55. Hodell DA, Williams DF, Kennett JP (1985) Late Pliocene reorganization of deep vertical water-mass structure in the western South Atlantic: Faunal and isotopic evidence. *Geol Soc Am Bull* 96:495–503.
56. Hodell DA, Venz-Curtis KA (2006) Late Neogene history of deepwater ventilation in the Southern Ocean. *Geochem Geophys Geosyst* 7:Q09001.
57. Mix AC, et al. (1995) Benthic foraminifer stable isotope record from Site 849 (0–5 Ma): Local and global climate changes. *Proc ODP Sci Results* 138:371–412.
58. Raymo ME, Ruddiman WF, Shackleton NJ, Oppo DW (1990) Evolution of Atlantic-Pacific $\delta^{13}C$ gradients over the last 2.5 m.y. *Earth Planet Sci Lett* 97:353–368.
59. Martinez-Garcia A, et al. (2011) Southern Ocean dust-climate coupling over the past four million years. *Nature* 476:312–315.
60. Becquey S, Gersonde R (2002) Pasthydrographic and climatic changes in the Subantarctic Zone of the South Atlantic-The Pleistocene record from ODP Site 1090. *Palaeogeog Palaeoclimat Palaeoecol* 182:221–239.
61. Bard E, Rickaby REM (2009) Migration of the subtropical front as a modulator of glacial climate. *Nature* 460:380–383.
62. Sijp WP, England MH (2009) Southern hemisphere westerly wind control over the ocean's thermohaline circulation. *J Clim* 22:1277–1286.
63. Lawrence KT, Liu Z, Herbert TD (2006) Evolution of the eastern tropical Pacific through Plio-Pleistocene glaciation. *Science* 312:79–83.
64. Marlow JR, Lange CB, Wefer G, Rosell-Mele A (2000) Upwelling intensification as part of the Pliocene-Pleistocene climate transition. *Science* 290:2288–2291.
65. Steph S, et al. (2010) Early Pliocene increase in thermohaline overturning: A precondition for the development of the modern equatorial Pacific cold tongue. *Paleoceanography* 25:PA2202.
66. Muratli JM, Chase Z, Mix AC, McManus J (2010) Increased glacial-age ventilation of the Chilean margin by Antarctic intermediate water. *Nat Geosci* 3:23–26.
67. Lee S, Poulsen CJ (2006) Sea ice control of Plio-Pleistocene tropical Pacific climate evolution. *Earth Planet Sci Lett* 248:253–262.
68. Chiang JCH, Bitz CM (2005) Influence of high latitude ice cover on the marine Intertropical Convergence Zone. *Climate Dynamics* 25:477–496.
69. Lee S, Chiang JCH, Matsumoto K, Tokos KS (2011) Southern Ocean wind response to North Atlantic cooling and the rise in atmospheric CO_2: Modeling perspective and paleoceanographic implications. *Paleoceanography* 26:PA1214.